Research Article | Vol. 25, No. 23 | 13 Nov 2017 | OPTICS EXPRESS 29380
Optics EXPRESS

Refractive index sensing using disk-hole coupling plasmonic structures fabricated on fiber facet

SHIJIE LI[1,2] AND WEN-DI LI[1,2,3*]

[1]*Department of Mechanical Engineering, the University of Hong Kong, Pokfulam, Hong Kong, China*
[2]*HKU-Zhejiang Institute of Research and Innovation (HKU-ZIRI), Hangzhou, Zhejiang 311300, China*
[3]*HKU-Shenzhen Institute of Research and Innovation (HKU-SIRI), Shenzhen, Guangdong 518000, China*
**liwd@hku.hk*

Abstract: We report a cost-effective and high-throughput method, featuring a double-transfer process and through-fiber curing, to pattern metallic nanostructures on optical fiber facet as portable plasmonic probes for refractive index (RI) sensing. A thin layer of ultraviolet-curable adhesive is coated onto fiber facet to imprint-transfer pre-fabricated metallic nanostructures from a polymeric template to the fiber facet. The reflection spectra of the plasmonic fiber probe in liquid solution samples with various RI are experimentally investigated to demonstrate its capability for real-time and in situ RI sensing. The optical reflection and local electric field distribution of the plasmonic sensing structures are also investigated through numerical modeling. The fiber-facet plasmonic sensor exhibits robust and flexible potential for RI-based sensing applications, and the reported fabrication method is applicable for the production of other functional nanodevices on fiber facets.

OCIS codes: (060.2370) Fiber optics sensors; (280.4788) Optical sensing and sensors; (220.4241) Nanostructure fabrication; (240.6680) Surface plasmons; (310.3840) Materials and process characterization.

References and links

1. O. Limaj, D. Etezadi, N. J. Wittenberg, D. Rodrigo, D. Yoo, S.-H. Oh, and H. Altug, "Infrared plasmonic biosensor for real-time and label-free monitoring of lipid membranes," Nano Lett. **16**(2), 1502–1508 (2016).
2. A. G. Brolo, "Plasmonics for future biosensors," Nat. Photonics **6**, 709–713 (2012).
3. F. Geiss, S. Fossati, I. Khan, N. G. Quilis, W. Knoll, and J. Dostálek, "UV-SPR biosensor for biomolecular interaction studies," in *SPIE Optics + Optoelectronics*, (International Society for Optics and Photonics, 2017), 1023107–1023108.
4. P. Jia, H. Jiang, J. Sabarinathan, and J. Yang, "Plasmonic nanohole array sensors fabricated by template transfer with improved optical performance," Nanotechnology **24**(19), 195501 (2013).
5. M. E. Stewart, N. H. Mack, V. Malyarchuk, J. A. Soares, T.-W. Lee, S. K. Gray, R. G. Nuzzo, and J. A. Rogers, "Quantitative multispectral biosensing and 1D imaging using quasi-3D plasmonic crystals," Proc. Natl. Acad. Sci. U.S.A. **103**(46), 17143–17148 (2006).
6. J. Homola, S. S. Yee, and G. Gauglitz, "Surface plasmon resonance sensors: review," Sensor Actuat. Biol. Chem. **54**, 3–15 (1999).
7. A. Tittl, H. Giessen, and N. Liu, "Plasmonic gas and chemical sensing," Nanophotonics **3**, 157–180 (2014).
8. R. Verma and B. D. Gupta, "Detection of heavy metal ions in contaminated water by surface plasmon resonance based optical fibre sensor using conducting polymer and chitosan," Food Chem. **166**, 568–575 (2015).
9. J.-F. Masson, "Surface plasmon resonance clinical biosensors for medical diagnostics," ACS Sens **2**(1), 16–30 (2017).
10. Z. S. Ballard, D. Shir, A. Bhardwaj, S. Bazargan, S. Sathianathan, and A. Ozcan, "Computational Sensing Using Low-Cost and Mobile Plasmonic Readers Designed by Machine Learning," ACS Nano **11**(2), 2266–2274 (2017).
11. B. Lee, S. Roh, and J. Park, "Current status of micro-and nano-structured optical fiber sensors," Opt. Fiber Technol. **15**, 209–221 (2009).
12. M. Consales, A. Ricciardi, A. Crescitelli, E. Esposito, A. Cutolo, and A. Cusano, "Lab-on-fiber technology: toward multifunctional optical nanoprobes," ACS Nano **6**(4), 3163–3170 (2012).
13. A. Ricciardi, M. Consales, G. Quero, A. Crescitelli, E. Esposito, and A. Cusano, "Lab-on-fiber devices as an all around platform for sensing," Opt. Fiber Technol. **19**, 772–784 (2013).

#305544 https://doi.org/10.1364/OE.25.029380
Journal © 2017 Received 25 Aug 2017; revised 11 Oct 2017; accepted 11 Oct 2017; published 9 Nov 2017

Optics EXPRESS

14. A. Ricciardi, A. Crescitelli, P. Vaiano, G. Quero, M. Consales, M. Pisco, E. Esposito, and A. Cusano, "Lab-on-fiber technology: a new vision for chemical and biological sensing," Analyst (Lond.) **140**(24), 8068–8079 (2015).
15. H.-H. Jeong, N. Erdene, S.-K. Lee, D.-H. Jeong, and J.-H. Park, "Fabrication of fiber-optic localized surface plasmon resonance sensor and its application to detect antibody-antigen reaction of interferon-gamma," Opt. Eng. **50**, 124405 (2011).
16. M. Pisco, F. Galeotti, G. Quero, A. Iadicicco, M. Giordano, and A. Cusano, "Miniaturized sensing probes based on metallic dielectric crystals self-assembled on optical fiber tips," ACS Photonics **1**, 917–927 (2014).
17. Y. Lin, Y. Zou, and R. G. Lindquist, "A reflection-based localized surface plasmon resonance fiber-optic probe for biochemical sensing," Biomed. Opt. Express **2**(3), 478–484 (2011).
18. M. Sanders, Y. Lin, J. Wei, T. Bono, and R. G. Lindquist, "An enhanced LSPR fiber-optic nanoprobe for ultrasensitive detection of protein biomarkers," Biosens. Bioelectron. **61**, 95–101 (2014).
19. Z. Zhang, Y. Chen, H. Liu, H. Bae, D. A. Olson, A. K. Gupta, and M. Yu, "On-fiber plasmonic interferometer for multi-parameter sensing," Opt. Express **23**(8), 10732–10740 (2015).
20. X. Lan, B. Cheng, Q. Yang, J. Huang, H. Wang, Y. Ma, H. Shi, and H. Xiao, "Reflection based extraordinary optical transmission fiber optic probe for refractive index sensing," Sensor Actuat. Biol. Chem. **193**, 95–99 (2014).
21. H. Nguyen, F. Sidiroglou, S. Collins, T. Davis, A. Roberts, and G. Baxter, "A localized surface plasmon resonance-based optical fiber sensor with sub-wavelength apertures," Appl. Phys. Lett. **103**, 193116 (2013).
22. A. Micco, A. Ricciardi, M. Pisco, V. La Ferrara, and A. Cusano, "Optical fiber tip templating using direct focused ion beam milling," Sci. Rep. **5**, 15935 (2015).
23. P. Jia, Z. Yang, J. Yang, and H. Ebendorff-Heidepriem, "Quasiperiodic Nanohole Arrays on Optical Fibers as Plasmonic Sensors: Fabrication and Sensitivity Determination," ACS Sensors **1**, 1078–1083 (2016).
24. P. Jia and J. Yang, "A plasmonic optical fiber patterned by template transfer as a high-performance flexible nanoprobe for real-time biosensing," Nanoscale **6**(15), 8836–8843 (2014).
25. X. He, H. Yi, J. Long, X. Zhou, J. Yang, and T. Yang, "Plasmonic crystal cavity on single-mode optical fiber end facet for label-free biosensing," Appl. Phys. Lett. **108**, 231105 (2016).
26. Z. Lei, X. Zhou, J. Yang, X. He, Y. Wang, and T. Yang, "Second-order distributed-feedback surface plasmon resonator for single-mode fiber end-facet biosensing," Appl. Phys. Lett. **110**, 171107 (2017).
27. A. Khan, S. Li, X. Tang, and W.-D. Li, "Nanostructure transfer using cyclic olefin copolymer templates fabricated by thermal nanoimprint lithography," J. Vac. Sci. Technol. B **32**, 06FI02 (2014).
28. X. Lu, R. Wan, and T. Zhang, "Metal-dielectric-metal based narrow band absorber for sensing applications," Opt. Express **23**(23), 29842–29847 (2015).
29. Y. Qu, Q. Li, H. Gong, K. Du, S. Bai, D. Zhao, H. Ye, and M. Qiu, "Spatially and Spectrally Resolved Narrowband Optical Absorber Based on 2D Grating Nanostructures on Metallic Films," Adv. Opt. Mater. **4**, 480–486 (2016).

1. Introduction

The development of plasmonic devices for various chemical and biological sensing applications has received increasing attention [1, 2]. Surface plasmon resonance (SPR) occurs in plasmonic sensors when light interacts with free electrons in the noble metal and can be observed in the far-field spectrum in the ultraviolet (UV) [3], visible [4] and infra-red regions [5]. Responses to changes in the local refractive index (RI), which modulates SPR conditions, can be tracked through the appearance of a characteristic peak or dip in the reflection or transmission spectrum of the device [6]. The spectral SPR response of the sensor is sensitive to surrounding environment or surface-binding events, thus making the sensor a potential platform for the real-time and label-free detection of gas leakage [7], water pollutant concentration [8], and disease diagnosis [9]. Research and development have focused on device miniaturization of plasmonic sensors for the production of portable and cost-effective devices to enable the practical applications of SPR sensing [10].

Quartz optical fiber is an intrinsically light-guiding substrate and is compatible with most s environment [11]. Therefore, it has the potential to act as a platform for SPR and many other sensing schemes. "Lab-on-fiber" technology has been proposed by Cusano et al [12–14] and various micro- and nanoscale functional structures have been constructed on fiber facet to make optical fiber itself a unique sensing device. There have been some attempts to apply conventional microfabrication techniques originally developed for planar substrates, such as nanoparticle self-assembly [15, 16], E-beam lithography [17, 18], and focused ion beam lithography [19–22], to fabricate nanostructures on optical fiber, however, to facilitate low-cost and high-throughput production of fiber-based plasmonic sensing devices, development

Optics EXPRESS

of improved fabrication methods is needed. Recently, the template transfer method has been developed to transfer functional nanostructures prefabricated on conventional substrates to fiber facet for plasmonic sensing functions [23–26]. Although excellent sensing performance has been achieved on carefully designed plasmonic structures [24-25], the fabrication process used in current work can be further developed to improve the efficiency, repeatability and accuracy for low-cost and mass-production of fiber-facet sensing devices. Particularly, compared with electron beam lithography patterning used in some of the existing works, nanoimprint lithography (NIL) is an ideal technique for its high-resolution and large patterning area, all desirable for large-quantity production.

In this paper, we report a fiber-facet RI sensor featuring disk-hole coupling plasmonic structure that is fabricated through a combined process of thermal NIL and UV-cured imprint transfer. Large-area plasmonic nanostructures are first fabricated on a polymeric intermediate template by thermal NIL and then transferred to bare optical fiber facet using a thin layer of UV-curable adhesive. A bi-layer plasmonic structure featuring gold disks and holes vertically separated by dielectric pillars is used as the sensing element because it can be fabricated in a facile one-step deposition process. We introduce a double-transfer process in the whole fabrication, which includes a first contact-transfer of a thin and uniform layer UV-curable adhesive and a second imprint-transfer of plasmonic sensing structures onto the fiber facet. Through-fiber UV-curing of the adhesive is used to simplify the fabrication process and improve fabrication throughput and utilization efficiency of the intermediate template. Since in our work only the bare optical fiber facet is in contact with the template, minimum area of prefabricated plasmonic structure is transferred to the fiber facet each time and the large-area template can be used to fabricate large quantity of fiber-based plasmonic probes in high-throughput production. The nanostructured fiber facet is finally characterized and demonstrated to be a portable RI sensor in reflection mode. The plasmonic structures on fiber facet are also numerically modeled using finite difference time domain (FDTD) method, to investigate the effect of various design parameters on the sensing performance.

2. Experiment and results

2.1 Fabrication of fiber-facet plasmonic sensor using nanoimprint and polymeric template transfer

Figure 1(a) shows the schematic of our fiber-facet plasmonic sensor. It contains a bi-layer disk-hole coupling plasmonic structure attached to the facet of optical fiber using a thin and uniform layer of UV-curable adhesive. The fabrication process for this plasmonic fiber probe is presented in Fig. 1(b)-1(g). The plasmonic sensing structures were first fabricated on a polymeric template using thermal NIL and thermal evaporation of gold. Silicon molds of 1 cm by 1cm large, carrying periodic nanoholes structures, were used to create nanopillar array structures on a cyclic olefin copolymer (COC) substrate using thermal NIL [27], as shown in Fig. 1(d). Details of the thermal NIL process were introduced previously [27] and COC was chosed owing to its low cost, low surface energy, chemical inertness, and high transparency. A thin layer of gold was then deposited on the nanopatterned COC substrate by thermal evaporation (Fig. 1(e)), forming a bilayer structure of coupled disks and holes in gold on the COC separated by COC pillars. The polymeric template with the bi-layer gold plasmonic structures will be used for subsequent transfer of plasmonic structures onto fiber facet.

We used bare quartz optical fiber with 200 μm core-diameter and 30 μm thick cladding layer in this work. The optical fiber was stripped and cleaved to obtain a flat tip for plasmonic structure transfer. The fiber facet needs to be further polished after cleavage to achieve high smoothness required by plasmonic structure fabrication. The cleaved bare fiber was inserted into a ferrule. Rosin was injected to the ferrule at elevated temperature and then cooled down to fix the fiber end in the ferrule. Standard polishing and grinding process was followed. Then the ferrule was heated again to melt the rosin and the polished fiber facet was pushed to

Optics EXPRESS

extrude out of the ferrule with approximately 1 cm length, ready for subsequent transfer of plasmonic nanostructures.

Double-transfer method was applied to transfer a thin and uniform layer of UV-curable adhesive on the fiber facet. Firstly, a drop of UV-curable adhesive (NOA 61, Norland Products, Inc.) was spin-coated on a carrying silicon substrate to form a thin film. Then the polished fiber facet was moved to be in contact with the adhesive film on the silicon substrate using a translation stage. The process was monitored by a microscopy camera and adjusted using manual tilting stages to achieve complete contact between the polished fiber facet and the silicon substrate. After separating the fiber facet from the silicon wafer, a thin and uniform layer of adhesive, with a thickness of approximately 20 μm was transferred onto the fiber facet, as shown in Fig. 1(b) and 1(c).

Then the fiber facet was moved to be in contact with the polymeric template with the bilayer gold structures using translation and tilting stages to ensure the fiber facet was perpendicularly pressed onto the polymeric template and the process was monitored by a microscopy camera, as shown in Fig. 1(f). UV-curing light was coupled into the fiber from its far end and delivered to the adhesive, exposing and curing the adhesive between fiber facet and the plasmonic structures on the polymeric template. After the adhesive being cured, the fiber probe was separated from the polymeric template with gold nanostructures transferred onto its facet. NOA 61 adhesive used in our work had strong chemical bond with metal and glass, and low adhesion with plastic substrate. This property contributed to the easy separation of the gold layer from its carrying polymeric template. All the fiber handling processes were carefully controlled by a custom-built 3D platform integrated with an LED source, motion-control stages, and monitoring microscopy cameras.

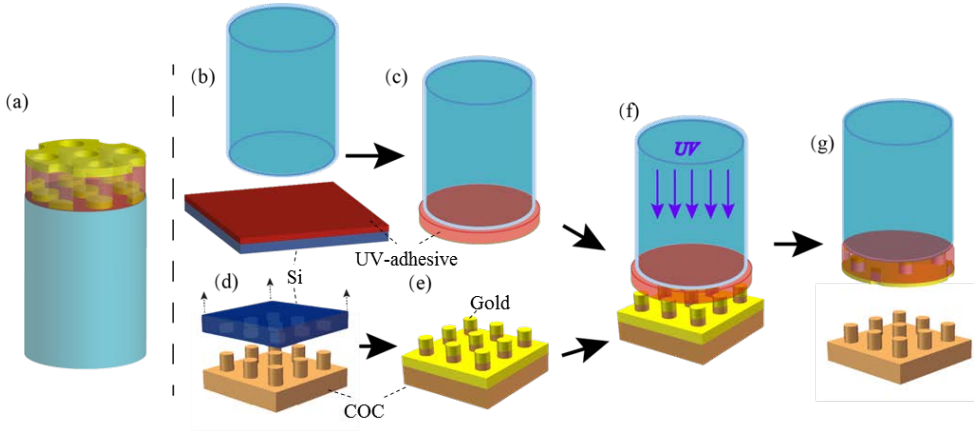

Fig. 1. Schematic of UV-cured imprint transfer process to fabricate nanostructures on optical fiber facet. (a) Final plasmonic fiber probe with coupling disk-hole bilayer gold structure patterned on top of fiber facet. (b) A thin layer of UV-curable adhesive spin-coated on a silicon wafer for adhesive transfer process. (c) Optical fiber with a thin layer of UV-curable adhesive transferred on the fiber facet. (d) Nanostructured COC template imprinted with nanopillar array on the surface through a thermal-NIL process. (e) COC template with evaporated gold layer. (f) UV-cured imprint-transfer process using exposing UV light delivered through the fiber. (g) Final fiber-facet plasmonic sensor with bilayer coupling plasmonic disk-hole array transferred on the surface.

2.2. Morphological characterization of the nanostructured fiber facet and its polymeric template

The side view images of the bare fiber tip before and after UV-cured imprint transfer are shown in Fig. 2(a). We fabricated two types of disk-hole coupling structures on fiber facet; one with gold hole-array on top and gold disks at the bottom of holes, as seen in Fig. 2(b) and 2(c), and the other with gold disks on top of pillars and gold hole array at the bottom, as seen

Optics EXPRESS

in Fig. 2(d) and 2(e). The nanostructured fiber facet shown in Fig. 2(c) features hexagonal hole-array on the surface of fiber facet with a gold layer thickness of 40 nm, hole diameter of 210 nm, and spacing of 600 nm. As shown in Fig. 2(e), a rectangular pillar-array with gold layer thickness of 100 nm, pillar diameter of 200 nm, and spacing of 600 nm was fabricated on the fiber facet. In Fig. 2(e), top gold disk-array is suspended on top of adhesive pillar-array, forming a dielectric spacing between the two gold layers. Moreover, the two SEM images shown in Fig. 2(b) and (d) prove that the self-guided fiber UV-curing process enables the confinement of adhesive curing within the fiber facet. This limited curing area eases the separation of the fiber facet from the template and simultaneously also improves the utilization of the intermediate template carrying plasmonic structures to be transferred.

Figure 2(f) presents the morphology of the 40 nm gold-coated COC template, which was used for fabrication of gold disk-hole coupling structures on the fiber facet shown in Fig. 2(b) and 2(c). As observed from the SEM image of the gold-coated COC template, disks have 220 nm diameters and are slightly larger than the holes fabricated on fiber facet shown in Fig. 2(c) because the lateral expansion of gold disks on the pillar top during evaporation deposition will gradually block the gold deposition on the bottom surface. Therefore, the holes on the optical fiber facet, which are the bottom gold layer on the COC template, are smaller than the disks in the holes. The pillar height of the COC template was measured by atom force microscopy (AFM) and is 162 nm, as shown in Fig. 2(f).

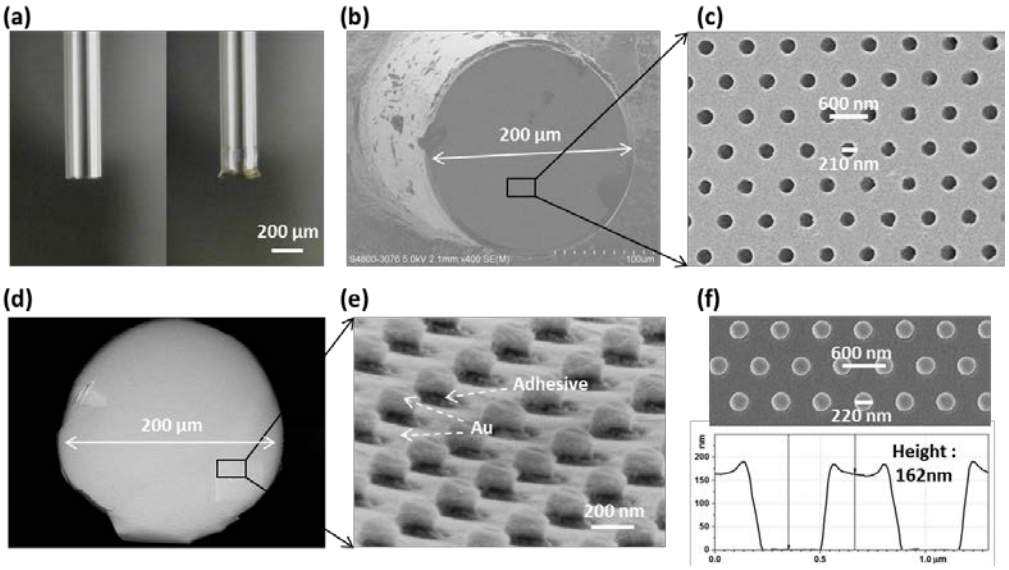

Fig. 2. (a) Side-view microscopy image of the optical fiber tip before (left) and after (right) UV-cured imprint transfer. (b) SEM images of the fiber probe facet covered by a gold hole-array. (c) Magnified detail of the SEM image of zoomed detail shown in (b). (d) SEM image of the fiber probe facet covered by a gold-coated pillar-array. (e) Magnified detail of the SEM image shown in (d). (f) COC template used for patterning the fiber facet shown in (b). The top SEM image shows its pillar-array nanostructure. The measurement of its height, which is 162 nm, is shown in the bottom AFM image.

2.3. Characterization and modeling of spectral reflectance of the fiber-facet plasmonic structure

We used the optical fiber with a hole-array (Fig. 2(b) and 2(c)) on its top surface as a plasmonic probe. To characterize its optical performance, reflection spectra were collected by delivering broadband illuminating light through the fiber to the plasmonic fiber facet using a halogen light source (HL-2000, Ocean Optics) and redirecting the reflected light through a bifurcated fiber to a spectrometer (HR2000 + CG, Ocean Optics). The measured reflectance

Optics EXPRESS

was normalized by using a fiber-optic reference mirror, which was fabricated by depositing a 200 nm-thick silver film on a 200 μm diameter multi-mode fiber facet. The measured reflection spectrum is plotted in Fig. 3(a) with a spectral dip at around 920 nm wavelength.

The reflection spectrum of the plasmonic fiber probe calculated through FDTD simulation (Lumerical Solutions Corp) is plotted and compared with the experimental results shown in Fig. 3(a). The incident plane wave propagates along the positive Z direction with E-field polarized in the X direction. The nanostructured fiber facet is placed in the X-Y plane with the fiber elongating in the negative Z direction. Periodic boundary conditions are applied to the X and Y directions, whereas perfectly matched layer (PML) boundary conditions are applied to the Z direction. A gradient mesh with the smallest size of 3 nm applied near the plasmonic structures is used in the modeling to ensure satisfactory balance between simulation accuracy and computing resource requirement.

The calculated reflection exhibits overall agreement with the experimental measurement. A narrower dip is observed in the simulated reflection spectrum mainly because the simulation uses a plane wave incident from the normal direction, while in the real sensor, the incident light has an angular distribution dependent on the fiber's numerical aperture. The spectral dip is associated with SPR behavior in the surface of the gold nanohole and nanodisk, as shown in the simulated local field distribution in Fig. 3(b), when the simulated E-field distribution is extracted at 920 nm wavelength in the X-Z plane. The E-field distribution in Fig. 3(b) indicates that the E-field is concentrated and enhanced in the air/gold and adhesive/gold interfaces, especially in the gold corners.

The SPR dip is sensitive to variations in the surrounding refractive indices. Thus, inserting a fiber tip into a media with a different RI will cause the reflection dip to shift accordingly. On the basis of this principle, the nanostructured optical fiber facet acts as a plasmonic probe for RI sensing.

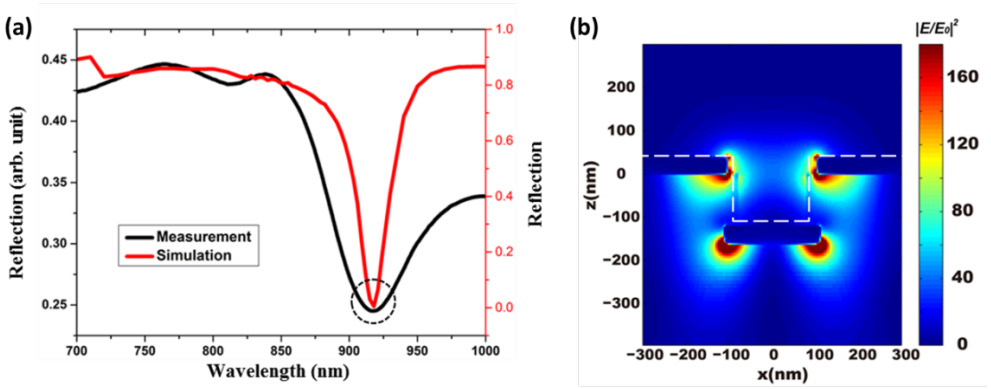

Fig. 3. (a) Comparison between the experimental and simulated reflection spectra of the plasmonic fiber probe. (b) Simulated electric field intensity distributions at 920 nm wavelength in the X-Z plane.

2.4. RI sensing using the plasmonic fiber-facet sensors

The applicability of the plasmonic fiber as a RI probe was assessed. The probe was immersed in a series of liquids with RI values of 1.328 to 1.450. Methanol, ethanol, and isopropyl alcohol (IPA) with RI values of 1.328, 1.362, and 1.378, respectively were used in the characterization. In addition, commercially available RI matching liquids (Cargille Company) with RI ranging from 1.40 to 1.45 with 0.01 interval were also used. After immersion in each RI liquid, the fiber probe was rinsed with isopropyl alcohol to remove residual RI liquid. The reflection spectra of plasmonic fiber tips immersed in different solutions were recorded from the measuring setup shown in Fig. 4(a). A fast Fourier transform based smoothing filter is applied to the original spectra to remove random high-frequency intensity noise and spectral

Optics EXPRESS

ripples. The smoothing filter does not alter the location of the spectral SPR dip. As the liquid index increases, the reflection spectrum red-shifts as shown in Fig. 4(b). Sensitivity (S) can be defined as the amount of wavelength shift $\Delta\lambda$ as a function of the induced RI change, with a unit of one nanometer per refractive index units (RIU):

$$S = \frac{\Delta\lambda}{RIU}, \tag{1}$$

where S is expressed in nm/RIU.

The SPR spectral dip wavelengths are plotted as a function of various RI, as shown in Fig. 4(c). A linear curve is drawn on the same figure to fit the experimental results and indicates that the S of the plasmonic fiber probe is 153 nm/RIU. FDTD simulation is carried out using background RI set to a series of values corresponding to the actual experiment. The simulated sensitivity derived from Fig. 4(d) is slightly higher than the measured value but is similar and also exhibits linear relation with the background RI.

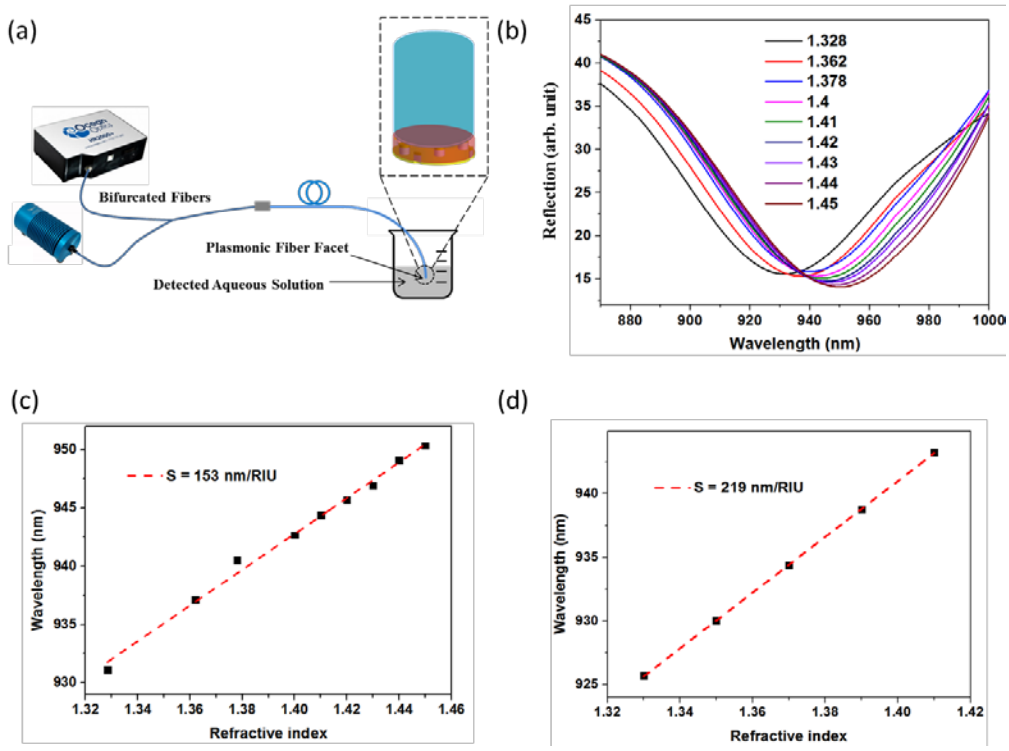

Fig. 4. (a) Optical setup for obtaining reflection spectra on the plasmonic fiber probe. (b) Measured reflection spectra of the fiber sensor in various RI solutions. (c) Relative wavelength shifts of the reflection dips as a function of the refractive index indicated in (b). (d) Simulated wavelength shifts of the reflection dip as a function of refractive index.

3. Discussion

3.1. Numerical investigation of local electric-field distribution on fiber-facet plasmonic structures with various geometric parameters

A series of FDTD simulations are conducted to investigate the correlation between the local E-field distributions and the geometry of the spaced gold nanostructures. The surrounding RI for modelling is set as 1.333, RI of deionized (DI) water. The pillar height on the COC template can be adjusted by setting different temperature and pressures during thermal-NIL.

Optics EXPRESS

The vertical spacing between the two gold layers of disks and holes on fiber facet can thus be modulated to optimize the sensing performance of the fiber-facet sensors. By enlarging the spacing, the local E-field intensity at the analyte/gold interface is strengthened, whereas the E-field intensity at gold/adhesive interface is weakened, as shown in Fig. 5(a). Experimentally, we chose 160 nm vertical spacing between the disks and holes to achieve reliable fabrication and reasonable E-field intensity distribution with major part of the E-field concentrated on the analyte/gold interface.

Local E-field distribution is also modeled to reveal the effect of varying gold layer thickness, as shown in Fig. 5(b). When the gold layer is thick (e.g., when the thickness is beyond 70 nm), the plasmonic fiber facet achieves weak E-field intensity at the analyte/gold interface, whereas the enhanced E-field is mostly focused to the bottom gold/adhesive interface. The thin gold layer generates a strong E-field for interaction with analyte solutions, but its thickness cannot be too thin to ensure enough reflective light intensity. We design the thickness of the gold layer to 40 nm to achieve balance between sensitivity and signal-to-noise ratio.

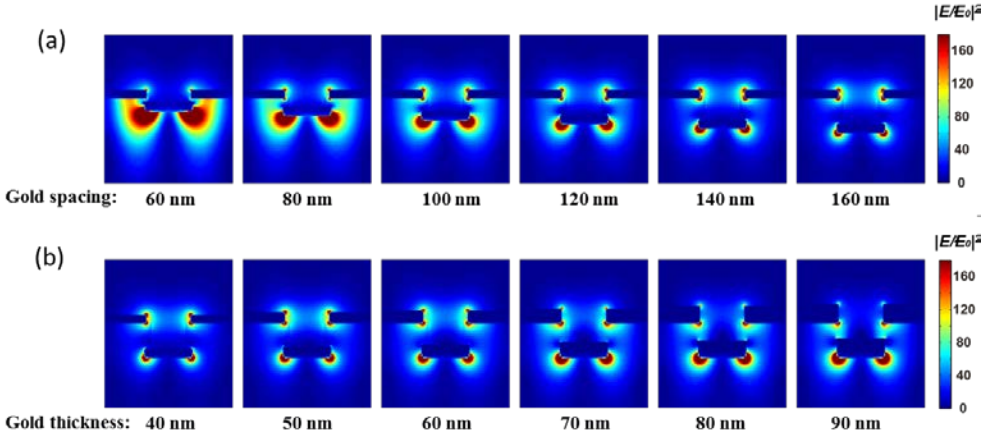

Fig. 5. Simulated local electric-field distribution as a function of (a) gold spacing on the fiber facet nanostructure (with the thickness of gold layer fixed at 40 nm) and (b) gold thickness on the fiber probe facet (with the spacing between the two layers fixed at 160 nm).

3.2. Temperature sensitivity of the spectral reflectance on fiber-facet plasmonic sensors

We performed the characterization of spectral reflectance on the fiber-facet plasmonic sensor in water under varying temperature to investigate its thermal stability and performance dependence on ambient temperature. A water tank was filled with DI water at 70 °C and the plasmonic fiber probe was immersed in the water. The room temperature was approximately 25 °C, and the reflection spectrum was taken for every 5 °C decrement in water temperature. The water temperature dropped rapidly at the initial stage and slowly decreased when it approached room temperature. A series of reflection spectra were recorded over time and are depicted in Fig. 6(a). The SPR dip wavelength was recorded and is plotted in Fig. 6(b). Linear curve fitting showed that the SPR dip was negatively correlated with temperature changes. The wavelength shift per °C was −137 pm because of RI and the volume changes of different layers on the nanostructured fiber facet. The equivalent RI deviation per °C local temperature change is calculated in accordance with Eq. (1) and is smaller than 0.0009 RIU, which corresponds to 9% error when 0.01 RIU resolution is expected during RI sensing experiment. This result proves that the plasmonic fiber-facet probe has a relatively insensitive dependence on the ambient temperature in a liquid environment.

Optics EXPRESS

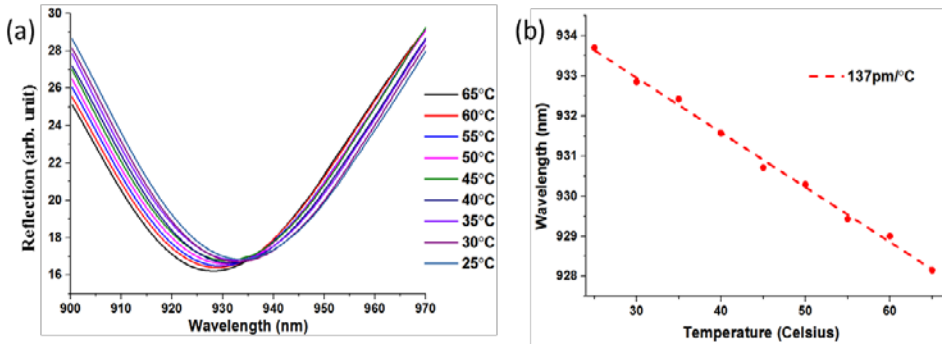

Fig. 6. (a) Extracted reflection spectra with temperature change. (b) Relative wavelength shifts of the reflection dip as a function of water temperature

4. Summary

We demonstrated a high-throughput and cost-effective fabrication scheme for patterning functional plasmonic nanostructures on fiber facets. The bi-layer gold disk-hole coupling structures fabricated on fiber facet are demonstrated in the application of in situ and real-time plasmonic sensing of refractive index. New processes introduced to the fabrication, including the double-transfer process for adhesive coating and plasmonic structure transferring and the through-fiber UV curing process, contributes to scalable, high-throughput, and low-cost fabrication of these fiber-facet plasmonic sensors. The reflection-based RI measurements using the fiber-facet plasmonic sensor were demonstrated to achieve 153 nm/RIU sensitivity with insensitive temperature dependence. The modeled local E-field distribution of the plasmonic fiber probes was analyzed to show the correlation between the plasmonic nanostructures' geometric profile and its local E-field distribution and help to choose structural parameters with rational design. We note that further improvement can be done on the fiber-facet refractometric sensors by adopting plasmonic structures with higher sensitivity [28-29]. The reflection-based fiber-facet plasmonic sensing probe is portable and has potential applications in point-of-care testing and the monitoring of environmental pollutants.

Funding

Research Grants Council of Hong Kong (HKRGC) (27205515, 17246116 and D-HK005/12T); Natural National Science Foundation of China (NSFC) (61306123); Science and Technology Innovation Commission of Shenzhen Municipality (JCYJ20140903112959959); Department of Science and Technology of Zhejiang Province (2017C01058); the University of Hong Kong (201611159284, 201611160057, 201511159175).

Acknowledgment

The authors thank Xinyu Wang for help on material deposition facility from Laboratory of Nanoscale Energy Conversion Devices and Physics at HKU.